

Implementation of synaptic learning rules by TaO⍰ memristors embedded with silver nanoparticles

Yue Ning(宁玥), Yunfeng Lai(赖云锋)†, Jiandong Wan(万建栋), Shuying Cheng(程树英), Qiao Zheng(郑巧), and Jinling Yu(俞金玲)

Citation: Chin. Phys. B, 2021, 30 (**4**): 047301. DOI: 10.1088/1674-1056/abccb8
Journal homepage: http://cpb.iphy.ac.cn; http://iopscience.iop.org/cpb

What follows is a list of articles you may be interested in

Digital and analog memory devices based on 2D layered MPS_3 (M=\,Mn, Co, Ni) materials

Guihua Zhao(赵贵华), Li Wang(王力), Xi Ke(柯曦), and Zhiyi Yu(虞志益)
Chin. Phys. B, 2021, 30 (**4**): 047303. DOI: 10.1088/1674-1056/abd397

Flexible and degradable resistive switching memory fabricated with sodium alginate

Zhuang-Zhuang Li(李壮壮), Zi-Yang Yan(严梓洋), Jia-Qi Xu(许嘉琪), Xiao-Han Zhang(张晓晗), Jing-Bo Fan(凡井波), Ya Lin(林亚), and Zhong-Qiang Wang(王中强)
Chin. Phys. B, 2021, 30 (**4**): 047302. DOI: 10.1088/1674-1056/abc67a

Review of resistive switching mechanisms for memristive neuromorphic devices

Rui Yang(杨蕊)
Chin. Phys. B, 2020, 29 (**9**): 097305. DOI: 10.1088/1674-1056/aba9c7

Effects of oxygen vacancy concentration and temperature on memristive behavior of $SrRuO_3$/Nb:$SrTiO_3$ junctions

Zhi-Cheng Wang(王志成), Zhang-Zhang Cui(崔璋璋), Hui Xu(徐珲), Xiao-Fang Zhai(翟晓芳), Ya-Lin Lu(陆亚林)
Chin. Phys. B, 2019, 28 (**8**): 087303. DOI: 10.1088/1674-1056/28/8/087303

Bias polarity-dependent unipolar switching behavior in NiO/$SrTiO_3$ stacked layer

Xian-Wen Sun(孙献文), Cai-Hong Jia(贾彩虹), Xian-Sheng Liu(刘献省), Guo-Qiang Li(李国强), Wei-Feng Zhang(张伟风)
Chin. Phys. B, 2018, 27 (**4**): 047304. DOI: 10.1088/1674-1056/27/4/047304

Implementation of synaptic learning rules by TaO_x memristors embedded with silver nanoparticles*

Yue Ning(宁玥), Yunfeng Lai(赖云锋)†, Jiandong Wan(万建栋), Shuying Cheng(程树英), Qiao Zheng(郑巧), and Jinling Yu(俞金玲)

School of Physics and Information Engineering, Fuzhou University, Fuzhou 350108, *China*

(Received 28 September 2020; revised manuscript received 12 November 2020; accepted manuscript online 23 November 2020)

As an alternative device for neuromorphic computing to conquer von Neumann bottleneck, the memristor serving as an artificial synapse has attracted much attention. The TaO_x memristors embedded with silver nanoparticles (Ag NPs) have been fabricated to implement synaptic plasticity and to investigate the effects of Ag NPs. The TaO_x memristors with and without Ag NPs are capable of simulating synaptic plasticity (PTP, STDP, and STP to LTP), learning, and memory behaviors. The conduction of the high resistance state (HRS) is driven by Schottky-emission mechanism. The embedment of Ag NPs causes the low resistance state (LRS) conduction governed by a Poole–Frenkel emission mechanism instead of a space-charge-limited conduction (SCLC) in a pure TaO_x system, which is ascribed to the Ag NPs enhancing electric field to produce additional traps and to reduce Coulomb potential energy of bound electrons to assist electron transport. Consequently, the enhanced electric fields induced by Ag NPs increase the learning strength and learning speed of the synapses. Additionally, they also improve synaptic sensitivity to stimuli. The linearity of conductance modulation and the reproducibility of conductance are improved as well.

Keywords: resistive switching, synaptic plasticity, memristor

PACS: 73.40.Rw, 77.80.Fm, 87.19.lg **DOI:** 10.1088/1674-1056/abccb8

1. Introduction

Due to the drawbacks of processing analog information, computing based on traditional von Neumann architectures is facing challenges in the era of information explosion.[1–4] Human brain has the advantages of low power consumption, high fault tolerance, and large-scale parallel processing ability to be a desirable candidate for processing analog information.[5–8] In a neuronal system, synapses connect neurons with its synaptic plasticity describing connection strength.[9] The improvement of synaptic plasticity will make the system more brain-like, and will further help to simulate complex neural functionalities.[10] Improving synaptic plasticity is thus essential for neuromorphic computing.[11]

A memristor, holding a sandwiched dielectric medium between electrodes, has a similar structure and functionalities to be an artificial counterpart of a biological synapse.[12–14] Tantalum oxide (TaO_x) exhibits good thermal stability, suitable dielectric constant, and excellent resistive switching properties to be regarded as a potential dielectric of the memristor-based artificial synapse.[15,16] An ideal artificial synapse should be able to simulate bio-synapse behaviors as much as possible. Fast processing speed, greater processing capability and desirable linearity of weight change might be welcome to the application of an artificial synapse.[17,18] Presenting synaptic weights with electrical conductance favors the imitation of synaptic behavior. The conductance of a memristor is closely associated with internal defects.[19] Resistive switching mechanism of a memristor is complex and under debate.[20–23] Several techniques have been attempted to modify defects in a memristor.[3,19,24] Adding metal nanoparticles into the dielectric might significantly affect defects in the memristor to modulate its resistive switching behavior,[25–27] suggesting a possible way to improve synaptic behaviors. However, systematic researches on the nanoparticle-modulating synaptic properties of a memristor are still rare. Considering the good electrochemical activity and low-cost, Ag nanoparticles were embedded into the TaO_x layer in this work to study the effects of Ag nanoparticles on resistive switching and synaptic behavior. The physical model was also proposed to understand the improvements in synaptic behavior.

2. Experimental details

Figure 1(a) shows a schematic diagram of a biological synapse with a TaO_x memristor as its artificial counterpart. To fabricate the TaO_x memristor, $\sim$ 15-nm TaO_x thin films were firstly sputter-deposited onto a p^+-Si bottom electrode (BE). Ultra-thin silver films were then deposited by thermal evaporation followed by 300-°C annealing for 3 min to form Ag nanoparticles (NPs). The morphologies of the Ag NPs covered surface are also shown in the inset of Fig. 1(b) with the

*Project supported by the National Natural Science Foundation of China (Grant No. 61674038), the Natural Science Foundation of Fujian Province, China (Grant No. 2019J01218), the Fund from the Fujian Science and Technology Innovation Laboratory for Optoelectronic Information of China (Grant No. 2021ZR145), and the Science Fund from the Fujian Provincial Department of Industry and Information Technology of China (Grant No. 82318075).

†Corresponding author. E-mail: Yunfeng.lai@fzu.edu.cn

© 2021 Chinese Physical Society and IOP Publishing Ltd

average Ag NPs diameter ∼ 11 nm. Subsequently, ∼ 15-nm TaO_x thin films were deposited on the Ag NPs to complete the deposition of dielectric layer. Finally, the ∼ 100-nm Ti top electrodes (TE) with a diameter of 75 μm were patterned to complete the fabrication of memristors. The TaO_x memristors without Ag NPs were also prepared for comparison.

The current–voltage (I–V) characteristics of the devices were measured by using a semiconductor parameter analyzer (4200-SCS; Keithley, USA). Synaptic behaviors of the devices were also characterized using the same system with the top electrode as the pre-synapse and the bottom electrode as the post-synapse.

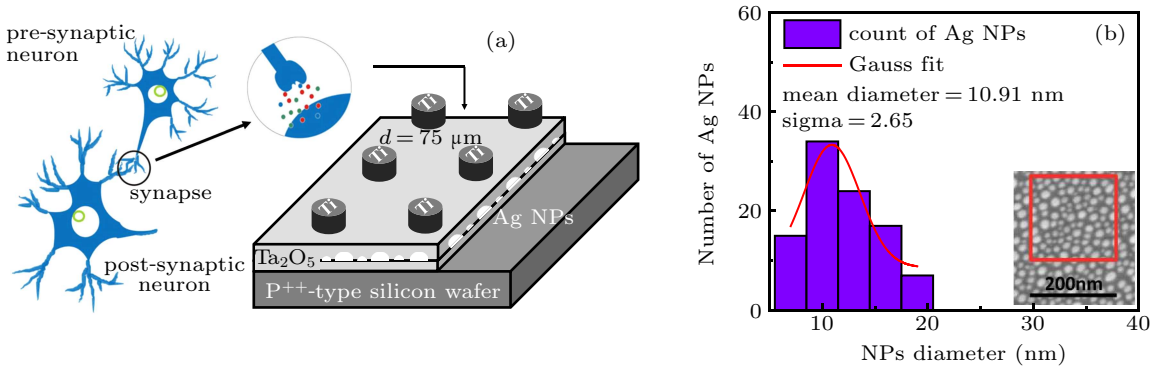


Fig. 1. (a) Schematic diagram of a biological synapse with a TaO_x memristor as its artificial counterpart. (b) The morphologies of the annealed Ag/TaO_x thin films (inset) with the size distribution of Ag NPs.

3. Results and discussion

3.1. Resistive switching

Resistive switching properties of the devices with and without Ag NPs were shown in Fig. 2. Resistance switches from a high resistance state (HRS) to a low resistance state (LRS) to finish a SET process if enough positive bias is applied [Fig. 2(a)]. However, it switches from the LRS back to the HRS to complete a RESET process when enough negative bias is applied.

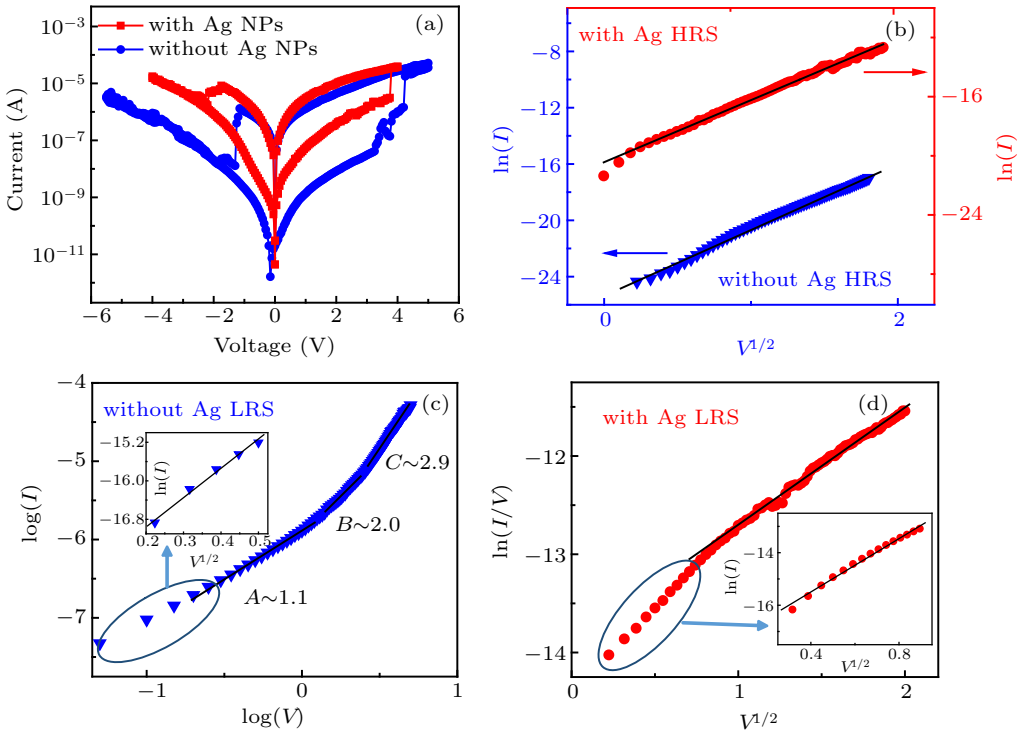


Fig. 2. Resistive switching characteristics of the memristors with and without Ag NPs. (a) I–V curves of the devices. (b) ln (I)–$V^{1/2}$ fittings for the HRSs of the devices. (c) log(I)–log(V) fitting for the LRS of the device without Ag NPs, the inset shows the ln(I)–$V^{1/2}$ fitting of the LRS under low voltage region. (d) ln(I/V)–$V^{1/2}$ fitting for the LRS of the device with Ag NPs, the inset shows the ln(I)–$V^{1/2}$ fitting of the LRS under low voltage region.

To understand the conduction mechanism of the devices, we replotted the current as a function of the applied positive voltages, as shown in Figs. 2(b)–2(d). As shown in Fig. 2(b), the linear fittings of ln(I) *versus* $V^{1/2}$ imply a Schottky-emission driven HRS conduction for the two devices.[22] In this case, electrons have to overcome the barrier at the Si/TaO_x

interface before getting into the TaO_x, and they finally reach the Ti electrode to complete transport. We, therefore, can observe a Schottky-emission driven conduction in the HRS. As the increasing electrical field produces more traps in the TaO_x to complete SET process, the device switches from an HRS to a LRS, exhibiting a space-charge-limited conduction (SCLC) for the memristor without Ag NPs due to three portions with different slopes (~ 1, ~ 2, and ~ 3) shown in Fig. 2(c).[28] However, the embedment of Ag NPs significantly changes the conduction mechanism of the LRS device. Figure 2(d) shows a well linear fitting of $\ln(I/V)$ *versus* $V^{1/2}$, which indicates that Poole–Frenkel emission dominates the conduction of the LRS of the Ag NPs embedded device. We could not deny Schottky-emission driven LRS conduction under low electric field, because the linear fittings of $\ln(I)$ *versus* $V^{1/2}$ in the insets of Figs. 2(c) and 2(d) might suggest Schottky-emission mechanism as well.

Figure 3 shows the energy diagram of the Ag NPs embedded devices with the parameters extracted from reference.[29] With the application of electric fields on the Ag NPs embedded device, a large number of traps generate to assist electron transport even at the lower voltages as the Ag NPs enhance the surrounding electric fields.[30] As a result, more traps are generated at a lower voltage to facilitate the conduction driven by a Poole–Frenkel emission mechanism instead of an SCLC mechanism. Additionally, the Coulomb potential energy of the bound electrons could be reduced as well to facilitate electron transport.[22] Compared with the current of a device without Ag NPs, the LRS current of a device with Ag NPs slightly increases, which further confirms the enhancement of electric fields by Ag NPs to produce additional traps.

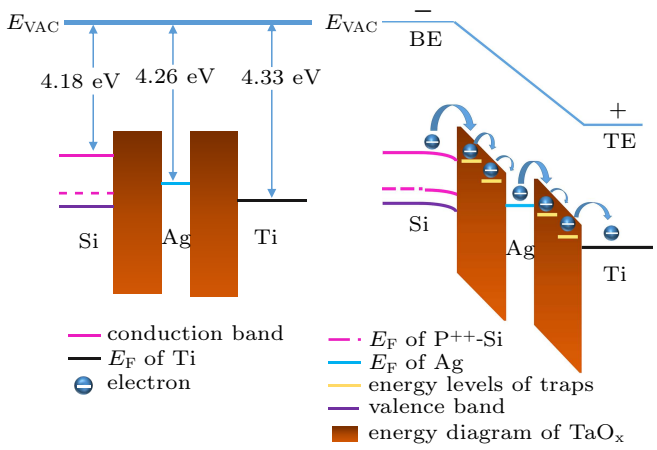


Fig. 3. Energy band diagrams of the Ag NPs embedded devices.

3.2. Synaptic plasticity and learning

In a biological system, the changes in synaptic strength can rapidly return to its initial state without sustaining stimulation, which is defined as short-term plasticity,[31] while if the synaptic strength is retained for a few hours or even a lifetime, long-term plasticity is available.[32] Long-term plasticity have been regarded as the basis of learning and memory.[33] Post-tetanic potentiation (PTP) characteristics as a kind of short-term plasticity, which corresponds to the enhancement effection on synaptic transmission efficiency after a series of repeated stimuli,[34] was mimicked by stimulating 10 electric pulses (amplitude = 2 V). The currents in response to the 1st and 10th stimulating pulses are marked as I_1 and I_{10}, respectively. Dependence of current change ($\Delta I = I_{10} - I_1$) on pulse interval is then presented in Fig. 4(a). The ΔI decreases with the increase of pulse interval, indicating the same tendency for the two devices. However, the ΔI margin of the Ag NPs embedded memristor is much larger, suggesting a larger learning strength by Ag NPs. The embedment of Ag NPs might take responsibility for the improvements. The enhanced electric fields by Ag NPs indeed increase the sensitivity of device to stimuli. The same stimuli usually trigger a much greater response for the Ag NPs embedded memristors. However, if the pulse interval extends, the traps excited by the enhanced electric fields might disappear before the arrival of next pulse. As a result, we can observe a greater margin for current modulation to favor a larger learning strength. Spike-timing-dependent plasticity (STDP) is a synaptic learning rule derived from biological Hebbian theory, which reflects the change of synaptic efficacy determined by the timing of the activity of pre- and post-neurons.[31] The synaptic weight changes (Δw) can be obtained by modulating the temporal difference (Δt) between pre- and post-synaptic spikes. Measurements were repeated three times for statistics. The relationship between Δw and Δt was calculated and the fitting formula is as follows:[35]

$$\Delta w = \begin{cases} A_+ \mathrm{e}^{-|\Delta t|/\tau_+}, & \Delta t > 0, \\ A_- \mathrm{e}^{-|\Delta t|/\tau_-}, & \Delta t < 0. \end{cases} \tag{1}$$

The Δw is defined as $(w_{\mathrm{post}} - w_{\mathrm{pre}})/w_{\mathrm{pre}}$, where the w_{pre} represents initial conductance and the w_{post} refers to the conductance after stimuli. $A_{+/-}$ and $\tau_{+/-}$ mean the learning scaling factors and the learning time constants of the exponential functions, respectively. As shown in Fig. 4(b), the stimuli of the pulse with width and interval of 20 ms were applied to the TE (pre-synapse) and the BE (post-synapse). When the pre-synaptic stimuli arrive earlier than the post-synaptic stimuli ($\Delta t > 0$), the synaptic weight is strengthened with the long-term potentiation (LTP). On the contrary, a decrease in synaptic weight would occur with long-term depression (LTD) if $\Delta t < 0$. Shorter temporal intervals lead to larger $|\Delta w|$ for both the potentiation and the depression processes. Ag NPs significantly extend the $|\Delta w|$ margin. The largest $|\Delta w|$ during the LTP process reaches $\sim 150\%$ instead of $\sim 30\%$ for the pure TaO_x memristor. The largest $|\Delta w|$ during the LTD process also increases to $\sim 80\%$. The embedment of Ag NPs extends learning strength of the memristor, which is consistent with the observations in Fig. 4(a). Additionally, both τ_+ and τ_- extracted

from the fitting curves slightly decrease, which suggests the embedded Ag NPs accelerate the learning speed of the device. It is known that the embedment of Ag NPs increases the surrounding electric fields even at a low voltage. Consequently, additional traps generate to shorten the distance between them under stimuli with even lower amplitude. Less displacement is required for those traps to reach another conductance state, and the memristor exhibits much faster learning speed.

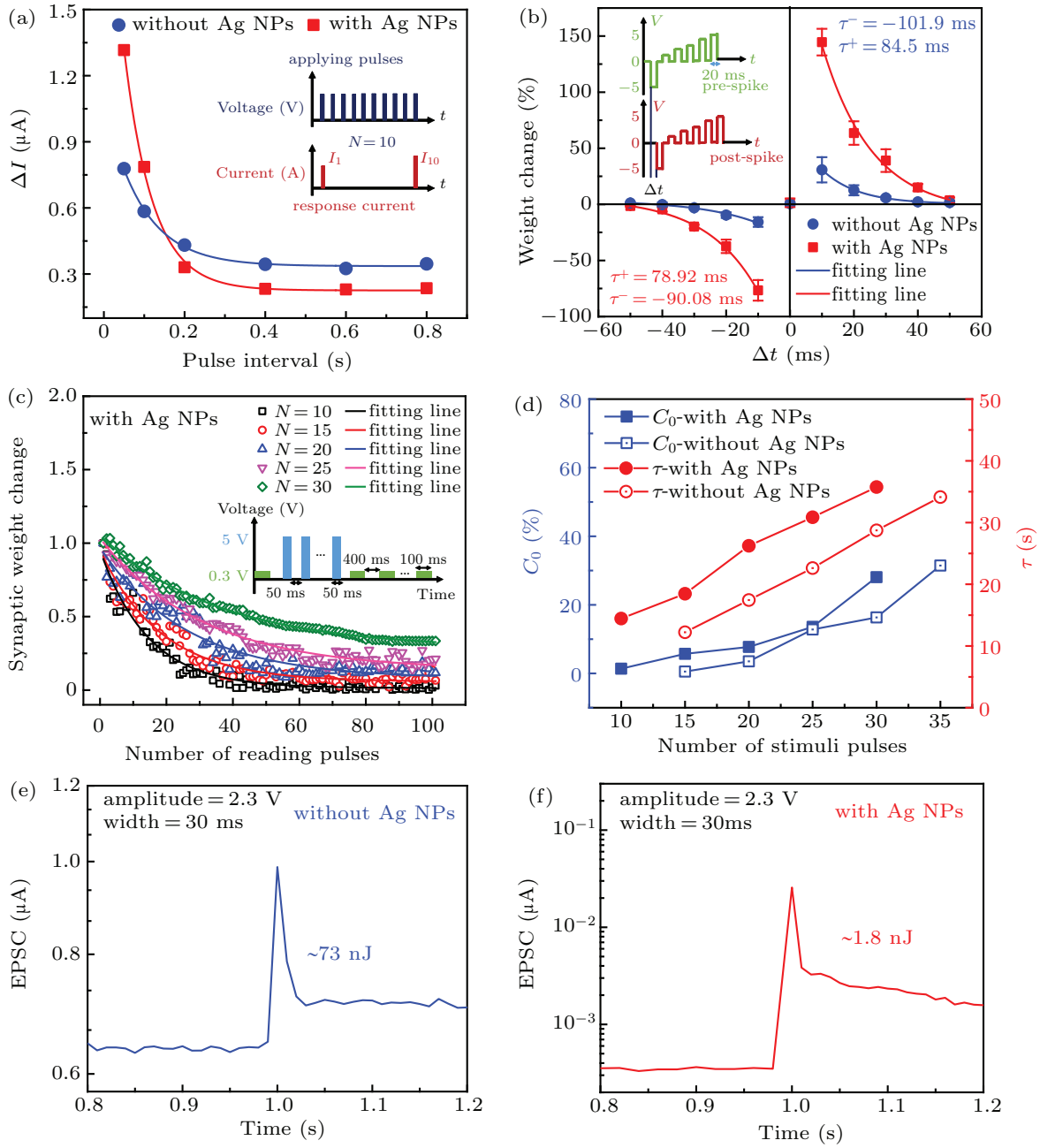


Fig. 4. Synaptic behaviors of the TaO_x memristors with and without Ag NPs. (a) PTP characteristics. The inset shows the pulse scheme and the response current. (b) STDP characteristics. The inset shows the pulse stimuli applied to the pre- and post-synapses. (c) Conductance change of the Ag NPs-embedded memristor after different numbers of stimuli. The inset shows the exciting (blue) and reading (green) pulse schemes. (d) Relationship between the correlation factor C_0, relaxation time τ, and exciting pulse number during the transition from STP to LTP. EPSC of our devices without (e) and with (f) Ag NPs at an input presynaptic pulse of 2.3 V at 30 ms.

Transformation from short-term plasticity (STP) to long-term plasticity (LTP) is essential for the learning and memory process.[36] Different numbers (N) of exciting pulses were applied to the devices to simulate the transformation. As the pulse scheme shown in the inset of Fig. 4(c), initial conductance was acquired by a 0.3-V reading pulse, followed by 5-V exciting pulses (width = 50 ms, interval = 50 ms, and N = 10, 15, 20, 25, 30, or 35) to perform LTP. Once the exciting stimuli were removed, 100 reading pulses (amplitude = 0.3 V, width = 100 ms, and interval = 400 ms) were applied to acquire conductance. The dependence of normalized synaptic weight change on the number of reading pulses are illustrated in Fig. 4(c). The decrease in conductance represents the forgetting process, and the Hermann Ebbinghaus's

forgetting curves were fitted to discover the long-term learning ability and forgetting speed. The normalized conductance changes and the forgetting curves were fitted according to $C = C_0 + A \cdot \exp(-t/\tau)$,[36,37] where C_0 and A are the correlation factors. The forgetting amount and forgetting speed decrease with the increase of C_0 and τ, which actually represent the normalized initial conductance and the relaxation time during the forgetting process, respectively. The C_0 and τ under different N were extracted and shown in Fig. 4(d). The C_0 and τ show an increasing trend with the increase in exciting pulse number, which indicates the transformation from STP to LTP. The embedment of Ag NPs increases C_0 and τ of the device, which implies that the Ag NPs can effectively enhance the memory strength of the TaO_x memristor and reduce its forgetting speed. The enhanced electric field by Ag NPs produces additional traps in the TaO_x to consolidate the connections in between, which indeed enhances the memory strength to reduce forgetting amount and to slow down forgetting.

Excitatory postsynaptic current (EPSC) stimulated by presynaptic potential spike is the response current. The EPSC of the devices without and with Ag NPs are respectively shown in Figs. 4(e) and 4(f). The energy to complete the spiking event is ~ 73 nJ for the device without Ag NPs, while the required energy is reduced to be ~ 1.8 nJ by the embedment of Ag NPs.

As a necessary functionality of a bio-synapse, the learning rule of the devices was simulated and shown in Fig. 5. Pulses are schematically shown in Fig. 5(a) with the blue pulses for stimulating the device and the green pulses for reading weight (or conductance) of the device. The weight change was calculated according to $\Delta w_{\text{learning}} = [(I_t - I_0)/I_0] \times 100\%$, where I_0 represents the initial current, I_t represents the current at any time during one learning process. While the forgetting curves were fitted by $\Delta w_{\text{forgetting}} = w_0 + A \cdot \exp(-t/\tau)$,[36] in which the w_0 represents memory capacity, and the τ again represents relaxation time during the forgetting process. As shown in the figures, gradually increased weight changes are available during the learning process. Then the pulses are removed to mimic the forgetting behavior. Memory capacity reaches a stable level after the first forgetting stage. It takes less number (26–30) of pulses to get 100% weight change to complete the second learning stage, indicating an increased learning speed. Meanwhile, memory capability increases further at the second forgetting stage. A tiny number (4–5) of pulses are required to obtain a 100% weight change during the third learning stage. The above observations suggest that the high-efficiency learning modes of experiential learning are successfully implemented. The values of w_0 and τ are extracted and marked in Fig. 5(b) to analyze the role of Ag NPs on learning. Ag NPs have neglectful effects on the w_0 due to quite similar values. However, Ag NPs remarkably increase the relaxation time from 2.73 s to 29.23 s with 9.7 times increasement during the first forgetting stage. The relaxation time is even extended 14.2 times during the second forgetting stage. Consequently, Ag NPs can consolidate the memory strength of the devices by decreasing forgetting speed, which well agrees with the observations in Fig. 4.

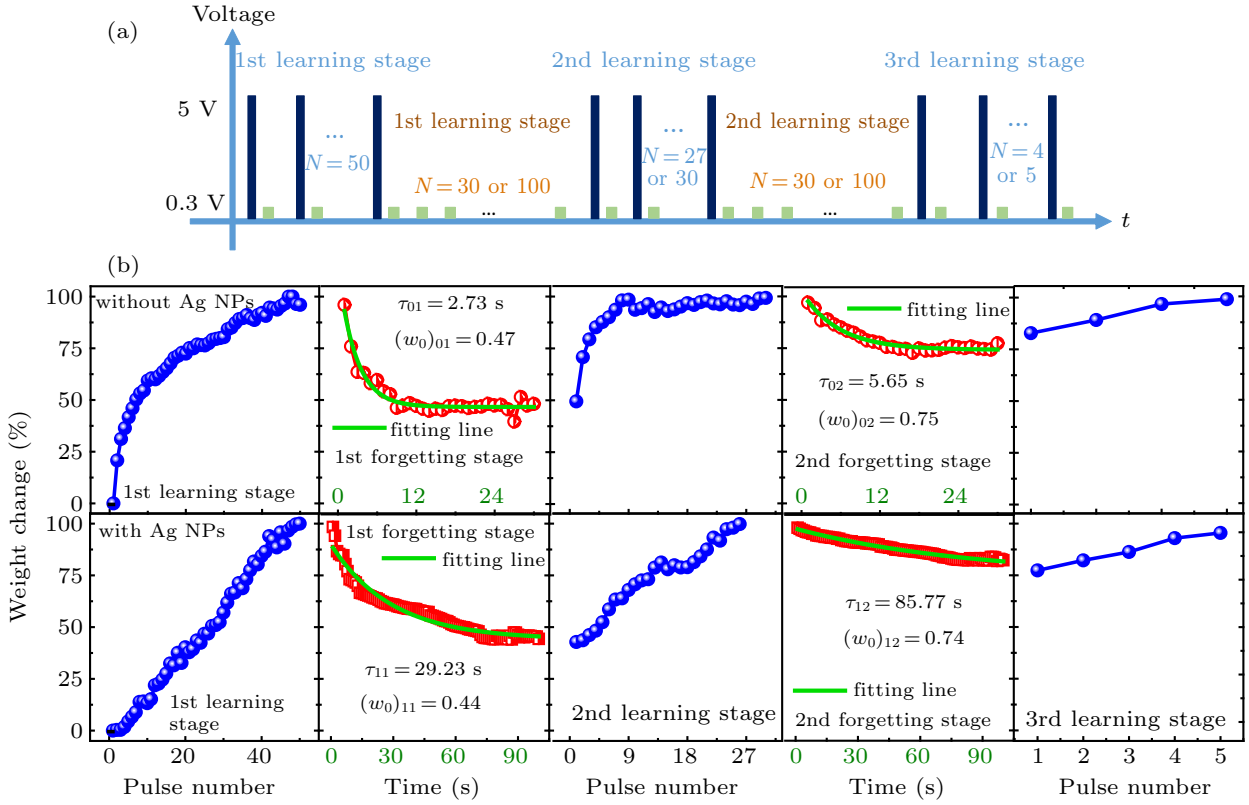


Fig. 5. Simulation of learning and forgetting processes of the two devices. (a) Pulse scheme for simulating learning with black pulses for stimulating and green ones for reading. (b) Simulation of learning and forgetting processes.

3.3. Linearity of conductance modulation

The long-term characteristics of the devices are also important. The stimulating pulse scheme is schematically depicted in Fig. 6(a). The dependence of conductance change on pulse number is shown in Fig. 6(b) with the curves fitted by the following formula:[38]

$$G = \begin{cases} a - c\mathrm{e}^{-\beta t}, & (\mathrm{LTP}), \\ a + c\mathrm{e}^{-\beta t}, & (\mathrm{LTD}), \end{cases} \tag{2}$$

where G represents device conductance, t represents testing time, a and c are fitting parameters, β is an exponential factor to reflect the degree of deviation from linearity during the conductance modulation process. A small value of β, indicating better linearity, is welcome for the practical applications of the electronic synapse.[38] To further estimate the reproducibility of the devices, the LTP and LTD repeat five times and the acquired β presents in Fig. 6(c). The β and its deviation are significantly decreased by Ag NPs during the LTP and LTD, which implies that the embedment of Ag NPs improves not only the linearity of conductance modulation but also reproducibility of the performance. The enhanced electric field by Ag NPs produces additional traps scattering in the TaO_x to assist electron transport. Stimuli in smaller amplitude are able to trigger slight displacement of the traps to reach an intermediate conductance state. We could observe small conductance modulations in response to small increase in stimuli amplitude, exhibiting improved conductance linearity for the potentiation and depression processes. Also, additional traps in a large number suppress the effects of individual stochastic movements of traps on performance. Reproducibility of the memristor might be increased as well.

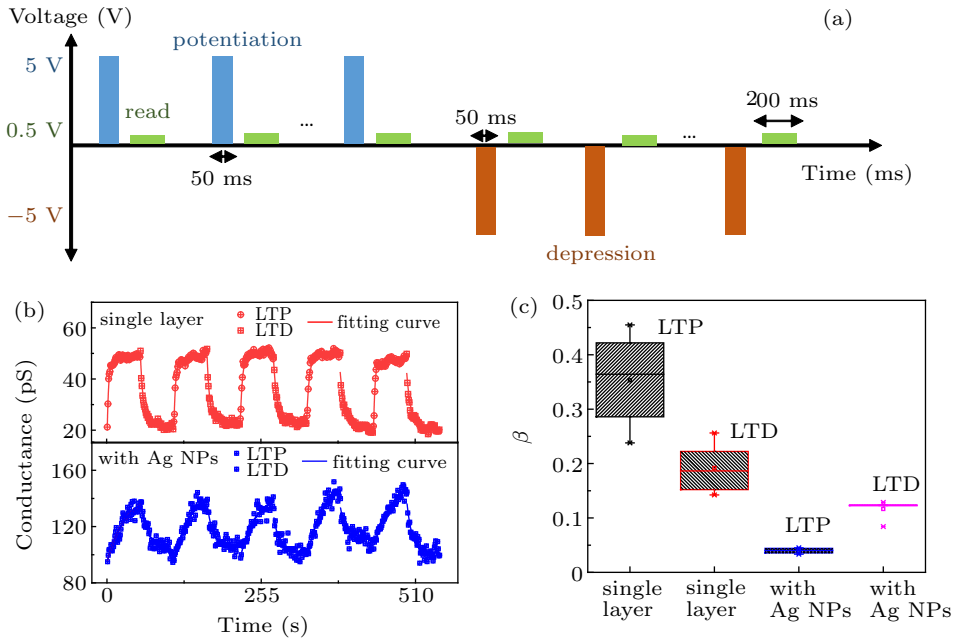


Fig. 6. Conductance modulation processes by stimuli. (a) Potentiating (in blue) and depressing (in red) pulse scheme. (b) Repeated conductance modulation during the LTP and LTD processes for the memristors with and without Ag NPs. (c) Comparison of β during the LTP and LTD processes.

4. Conclusions

The Ag NPs-embedded TaO_x memristors have been fabricated with a Poole–Frenkel emission governed conduction in the LRS and a Schottky-emission driven conduction in the HRS. The TaO_x memristors with and without Ag NPs are able to serve as artificial synapses to implement synaptic plasticity, learning and memory functions. The embedded Ag NPs improve synaptic performance of the device with a larger learning strength and faster learning speed. Additionally, the embedded Ag NPs significantly improve the linearity of conductance modulation and reproducibility of the devices. The enhanced electric fields by Ag NPs to produce additional traps are believed to be responsible for the above improvements.

References

[1] Merolla P A, Arthur J V, Alvarez-Icaza R, Cassidy A S, Sawada J, Akopyan F, Jackson B L, Imam N, Guo C, Nakamura Y, Brezzo B, Vo I, Esser S K, Appuswamy R, Taba B, Amir A, Flickner M D, Risk W P, Manohar R and Modha D S 2014 *Science* **345** 668
[2] Zhou L, Mao J Y, Ren Y, Yang J Q, Zhang S R, Zhou Y, Liao Q F, Zeng Y J, Shan H Q, Xu Z X, Fu J J, Wang Y, Chen X L, Lv Z Y, Han S T and Roy V A L 2018 *Small* **14** 1800288
[3] Chandrasekaran S, Simanjuntak F M, Saminathan R, Panda D and Tseng T Y 2019 *Nanotechnology* **30** 445205
[4] Li Y, Zhong Y, Zhang J, Xu L, Wang Q, Sun H, Tong H, Cheng X and Miao X 2014 *Sci. Rep.* **4** 4906
[5] Wan Q Z, Sharbati M T, Erickson J R, Du Y H and Xiong F 2019 *Adv. Mater. Technol.* **4** 1900037
[6] Wang J R and Zhuge F 2019 *Adv. Mater. Technol.* **4** 1800544
[7] Li S Z, Zeng F, Chen C, Liu H Y, Tang G S, Gao S, Song C, Lin Y S, Pan F and Guo D 2013 *J. Mater. Chem. C* **1** 5292
[8] Waser R, Dittmann R, Staikov G and Szot K 2009 *Adv. Mater.* **21** 2632
[9] Zhu L Q, Wan C J, Guo L Q, Shi Y and Wan Q 2014 *Nat. Commun.* **5** 3158

[10] Li E L, Lin W K, Yan Y J, Yang H H, Wang X M, Chen Q Z, Lv D X, Chen G X, Chen H P and Guo T L 2019 *ACS Appl. Mater. Interfaces* **11** 46008

[11] Sabatini B L 2007 *Nature* **450** 1173

[12] Yu S M, Gao B, Fang Z, Yu H Y, Kang J F and Wong H S P 2013 *Adv. Mater.* **25** 1774

[13] Wang Z Q, Xu H Y, Li X H, Yu H, Liu Y C and Zhu X J 2012 *Adv. Funct. Mater.* **22** 2759

[14] Wang Z R, Joshi S, Savel'ev S E, Jiang H, Midya R, Lin P, Hu M, Ge N, Strachan J P, Li Z Y, Wu Q, Barne M, Li G L, Xin H L, Williams R S, Xia Q F and Yang J J 2017 *Nat. Mater.* **16** 101

[15] Kim J Y, Garg A, Rymaszewski E J and Lu T M 2001 *IEEE Trans. Compon. Packaging Technol.* **24** 526

[16] Chen C, Song C, Yang J, Zeng F and Pan F 2012 *Appl. Phys. Lett.* **100** 253509

[17] Ham S, Choi S, Cho H, Na S I and Wang G 2019 *Adv. Funct. Mater.* **29** 1806646

[18] Sung C, Lim S, Kim H, Kim T, Moon K, Song J, Kim J J and Hwang H 2018 *Nanotechnology* **29** 115203

[19] Wan J D, Qiu W B, Lai Y F, Lin P J, Zheng Q, Yu J L, Cheng S Y and Zhang H Z 2020 *J. Phys. D: Appl. Phys.* **53** 055303

[20] Tian J J, Wu H J, Fan Z, Zhang Y, Pennycook S J, Zheng D F, Tan Z W, Guo H Z, Yu P, Lu X B, Zhou G F, Gao X S and Liu J M 2019 *Adv. Mater.* **31** 1903679

[21] Fan Z, Fan H, Yang L, Li P L, Lu Z X, Tian G, Huang Z F, Li Z W, Yao J X, Luo Q Y, Chen C, Chen D Y, Yan Z B, Zeng M, Lu X B, Gao X S and Liu J M 2017 *J. Mater. Chem. C* **5** 7317

[22] Chiu F C 2014 *Adv. Mater. Sci. Eng.* **2014** 578168

[23] Lai Y F, Chen F, Zeng Z C, Lin P J, Cheng S Y and Yu J L 2017 *Chin. Phys. B* **26** 087305

[24] Lai Y F, Zeng Z C, Liao C H, Cheng S Y, Yu J L, Zheng Q and Lin P J 2016 *Appl. Phys. Lett.* **109** 063501

[25] Gogurla N, Mondal S P, Sinha A K, Katiyar A K, Banerjee W, Kundu S C and Ray S K 2013 *Nanotechnology* **24** 345202

[26] Son D I, Park D H, Kim J B, Choi J W, Kim T W, Angadi B, Yi Y and Choi W K 2011 *J. Phys. Chem. C* **115** 2341

[27] Khurana G, Misra P, Kumar N, Kooriyattil S, Scott J F and Katiyar R S 2016 *Nanotechnology* **27** 015702

[28] Liu Q, Guan W H, Long S B, Jia R, Liu M and Chen J N 2008 *Appl. Phys. Lett.* **92** 012117

[29] Shvets V A, Aliev V S, Gritsenko D V, Shaimeev S S, Fedosenko E V, Rykhlitski S V, Atuchin V V, Gritsenko V A, Tapilin V M and Wong H 2008 *J. Non-Cryst. Solids* **354** 3025

[30] Gao L W, Li Y H, Li Q, Song Z X and Ma F 2017 *Nanotechnology* **28** 215201

[31] Upadhyay N K, Joshi S and Yang J J 2016 *Sci. China-Inf. Sci.* **59** 061404

[32] Tang J S, Yuan F, Shen X K, Wang Z R, Rao M Y, He Y Y, Sun Y H, Li X Y, Zhang W B, Li Y J, Gao B, Qian H, Bi G Q, Song S, Yang J J and Wu H Q 2019 *Adv. Mater.* **31** 1902761

[33] Lynch M A 2004 *Physiol. Rev.* **84** 87

[34] Bao J X, Kandel E R and Hawkins R D 1997 *Science* **275** 969

[35] Froemke R C and Dan Y 2002 *Nature* **416** 433

[36] Chang T, Jo S H and Lu W 2011 *Acs Nano* **5** 7669

[37] Ebbinghaus H 2013 *Ann. Neurosci.* **20** 155

[38] Wang Z W, Yin M H, Zhang T, Cai Y M, Wang Y Y, Yang Y C and Huang R 2016 *Nanoscale* **8** 14015